Quantifying particle-to-particle heterogeneity in aerosol hygroscopicity

Liang Yuan[1, 2] and Chunsheng Zhao[2, *]

[1]Chengdu Plain Urban Meteorology and Environment Scientific Observation and Research Station of Sichuan Province,
School of Atmospheric Sciences, Chengdu University of Information Technology, Chengdu 610225, China
[2]Department of Atmospheric and Oceanic Sciences, School of Physics, Peking University, Beijing, 100871, China

Correspondence: Chunsheng Zhao (zcs@pku.edu.cn)

Abstract. The particle-to-particle heterogeneity in aerosol hygroscopicity is crucial for understanding aerosol climatic and environmental effects. The hygroscopic parameter κ, widely applied to describe aerosol hygroscopicity for aerosol populations both in models and observations, is a probability distribution highly related to aerosol heterogeneity due to the complex sources and aging processes. However, the heterogeneity in aerosol hygroscopicity is not represented in observations and model simula-

5 tions, leading to challenges in accurately estimating aerosol climatic and environmental effects. Here, we propose an algorithm for quantifying particle-to-particle heterogeneity in aerosol hygroscopicity, based on information-theoretic entropy measures, by using the data that comes only from the in-situ measurement of the hygroscopicity tandem differential mobility analyzer (H-TDMA). Aerosol populations in this algorithm are assumed to be simple binary systems consisting of the less hygroscopic and more hygroscopic components, which are commonly used in H-TDMA measurement. Three indices, including the aver-

10 age per-particle species diversity D_α, the bulk population species diversity D_γ, and their affine ratio χ, are calculated from the probability distribution of κ to describe aerosol heterogeneity. This algorithm can efficiently characterize the evolution of aerosol heterogeneity with time in the real atmosphere. Our results show that the heterogeneity varies much with aerosol particle size and large discrepancies exist in the width and peak value of particle number size distribution (PNSD) with varied heterogeneity after hygroscopic growth, especially for conditions with high relative humidity. This reveals a vital role of the

15 heterogeneity in ambient PNSD and significant uncertainties in calculating the climate-relevant properties if the population-averaged hygroscopicity is applied by neglecting its heterogeneity. This work points the way toward a better understanding of the role of hygroscopicity in evaluating aerosol climatic and environmental impacts.

1 Introduction

Aerosol hygroscopicity describes the interaction of aerosols and water vapor and severely influences aerosol climatic and

20 environmental effects (Wang and Chen, 2019; Swietlicki et al., 2008; Liu et al., 2013; Tie et al., 2017). It is highly related to the particle-to-particle heterogeneity in aerosol hygroscopicity, which is crucial but not considered in observations and models, posing a challenge in accurately estimating aerosol effects on climate and environment.

Köhler theory (Köhler, 1936) is the basis of the studies on aerosol hygroscopicity. Nowadays, the most widely used parameter to describe aerosol hygroscopicity in observations and models is the hygroscopicity parameter, κ, proposed in κ-Köhler theory

25   (Petters and Kreidenweis, 2007). κ extends and facilitates the application of Köhler theory (Zieger et al., 2013; Bian et al., 2014; Chen et al., 2014; Tao et al., 2014; Brock et al., 2016) and can be expediently observed under both subsaturated (Liu et al., 1978; Kuang et al., 2017) and supersaturated conditions (Petters and Kreidenweis, 2007; Cai et al., 2018). It can also be derived from the observed chemical composition (Liu et al., 2014). Considering that ambient aerosol particles in an aerosol population differ dramatically in chemical composition due to the complex sources and aging processes. In terms of aerosol

30   hygroscopicity, the distribution of the nearly hydrophobic (NH), the less hygroscopic (LH), and the more hygroscopic (MH) components (Liu et al., 2011; Tan et al., 2013b; Yuan et al., 2020) vary between and within particles. Such particle-to-particle heterogeneity in aerosol hygroscopicity results in a probability distribution of κ (κ-PDF) for an aerosol population. Among the three above-mentioned observing techniques, although the hygroscopicity tandem differential mobility analyzer (H-TDMA) can directly achieve κ-PDF under subsaturated condition, which is essential to investigate the hygroscopicity and activation

35   property of aerosol populations, most studies focus on the analysis and application of the population-averaged κ (κ_{mean}) by neglecting the heterogeneity (Chen et al., 2014; Tao et al., 2014; Brock et al., 2016; Kuang et al., 2017; Liu et al., 1978; Cai et al., 2018; Liu et al., 2014; Yuan et al., 2020; Wang et al., 2018), leading to uncertainties in the estimation of aerosol impacts on climate and environment.

    Many research fields face the problem of heterogeneity involving the diversity of variables or issues. The diversity is first

40   quantified in Whittaker (1972) by introducing the information-theoretic entropy in ecology and then in many other fields, including economics (Drucker, 2013), immunology (Tsimring et al., 1996), neuroscience (Strong et al., 1998), and genetics (Falush et al., 2007). Riemer and West (2013) applied it in atmospheric science for the research of aerosol mixing state. By referring to Whittaker (1972) and Riemer and West (2013) , the impact of the mixing state of black carbon (BC)-containing particles on light absorption enhancement is investigated, which shows that absorption is strongly affected by the heterogeneity of

45   BC-containing aerosol population and explains that the discrepancy between simulated and observed absorption enhancement accounts for the particle-to-particle heterogeneity in composition (Fierce et al., 2016, 2020; Zhao et al., 2021). How crucial the heterogeneity in aerosol hygroscopicity is for the highly climate-relevant aerosol size distribution, optical, and activation properties? However, to the best of the authors' knowledge, most literature is not focused on quantitatively evaluating the heterogeneity concerning aerosol hygroscopicity for in-situ measurements.

50   Given these considerations, we propose an algorithm for quantifying the particle-to-particle heterogeneity in aerosol hygroscopicity in the real atmosphere. This algorithm is based on information-theoretic entropy measures, employing observed data from the in-situ measurement of H-TDMA. In the following, section 2 will describe the detail of the algorithm; The interpretation of the results from the algorithm will be presented in section 3. The importance of the heterogeneity and the application of the algorithm are discussed and also included in section 3; The last section comes the conclusions.

2 Data and Methods

2.1 Measurement site

The campaign was implemented for two periods from 23 January to 25 February and 19 July to 8 September 2019, respectively, at the meteorological station (30.58°N, 103.98°E) inside the campus of Chengdu University of Information and Technology (CUIT) located in Shuangliu district, southwest of the main urban area of Chengdu, China. The elevation of the observation site is approximately 500 m. Fig. S1 in the supplemental file shows the map of the site. It is surrounded by residential neighbourhoods with no nearby sources of significant industrial pollution. Aerosol particles here are representative of the urban environments. More details can be found in Yuan et al. (2020)

2.2 Data of H-TDMA measurement

A custom-built H-TDMA designed by Tan et al. (2013a) is employed to obtain the hygroscopic properties for aerosols with dry diameters $D_p(\mathrm{Dry})$ of 40, 80, 110, 150, and 200 nm. The schematic structure of the H-TDMA is shown in Fig. S2 in the supplemental file. This H-TDMA is placed in a temperature-controlled (25 °C) container, with an aerosol inlet equipped with a $PM_{2.5}$ impactor that extends out of the container from the roof and set approximately 3 m above ground. It mainly consists of two differential mobility analyzers (DMA) (Model 3081A, TSI Inc., USA), a humidification system and a condensation particle counter (CPC) (Model 3787, TSI Inc., USA). Aerosol samples with a flow of $0.6\ \mathrm{L\cdot min^{-1}}$ are first introduced into a Nafion dryer (Model MD-700-24S-3, Perma Pure Inc., USA) by an external vacuum pump to maintain the RH below 10%. These aerosols flow through an advanced aerosol X-ray neutralizer (Model 3088, TSI Inc., USA) to be single-charged and are then screened by the first DMA (DMA1) with set voltages. Subsequently, the selected quasi-monodisperse dry aerosols feed into a Nafion humidifier (Model PD-07018T-24MSS, Perma Pure Inc., USA) with RH of 90% ($\pm$0.3%). Finally, the PNSDs of humidified particles out of the humidifier are measured by the second DMA (DMA2) coupled with the CPC. The details of the H-TDMA refer to Yuan et al. (2020).

The growth factor (g) of the quasi-monodisperse aerosols $g[D_p(\mathrm{Dry})]$ selected by the first differential mobility analyzer (DMA) equipped in the H-TDMA can be then calculated by:

$$g[D_p(\mathrm{Dry})] = \frac{D_p(\mathrm{RH})}{D_p(\mathrm{Dry})}, \tag{1}$$

where $D_p(\mathrm{RH})$ represents the particle diameter screened by DMA2 at a specific relative humidity (RH), e. g., 90% in this study. The measured distribution function of g (g-MDF) is calculated from aerosol particle number size distribution (PNSD) counted by the CPC installed downstream of the second DMA. The $\mathrm{TDMA_{fit}}$ algorithm (Stolzenburg and McMurry, 2008) is employed to convert the g-MDF to the actual probability distribution function (g-PDF) in the campaign (Gysel et al., 2009). For each measured dry diameter, the g-PDFs are thereafter normalized as:

$$\int c(g)\mathrm{d}g = 1, \tag{2}$$

where, $c(g)$ represents the normalized g-PDF. For each g, κ can be converted using κ-Köhler theory (Petters and Kreidenweis, 2007):

$$\kappa = (g^3 - 1) \times \left[\frac{1}{RH} \times \exp\left(\frac{4\sigma_{s/a}M_{\mathrm{w}}}{RT\rho_{\mathrm{w}}D_{\mathrm{p}}(\mathrm{Dry})g} \right) - 1 \right], \tag{3}$$

where $\sigma_{\mathrm{s/a}}$ of $0.072\,\mathrm{J\cdot m^{-2}}$ is the surface tension of the solution/air interface; M_{w} of $18.015\,\mathrm{g\cdot mol^{-1}}$ is the molecular weight of water; ρ_{w} of $1.0\,\mathrm{g\cdot cm^{-3}}$ is the density of water; R of $8.315\,\mathrm{J\cdot K^{-1}\cdot mol^{-1}}$ is the universal gas constant; T of 298.15 K is the temperature in Kelvin. Then, the κ-PDF can be obtained and normalized as:

$$\int c(\kappa)\mathrm{d}\kappa = 1, \tag{4}$$

where $c(\kappa)$ is the normalized κ-PDF as the examples shown in Fig. 1.

2.3 Calculation of the heterogeneity in aerosol hygroscopicity

The particle-to-particle heterogeneity in aerosol hygroscopicity is calculated by using the H-TDMA measured κ-PDF (e. g. the examples in Fig. 1). The key assumption is that an aerosol population containing N aerosol particles is a binary system consisting of the LH and MH components with respective κ of 0.01 (κ_{LH}) (typical for organics) and 0.6 (κ_{MH}) (typical for sulphate and nitrate). Each aerosol particle in the population contains one or two of the LH and MH components and thus their κ varied between 0.01 and 0.6. κ-PDF of the aerosol population can be considered as the normalized aerosol number fractions varied with κ between 0.1 and 0.6 (Fig. 1). The volume fraction of these two components in each aerosol particle can be calculated based on κ according to the ZSR rule (Zdanovskii, 1948; Stokes and Robinson, 1966).

By refering to information-theoretic entropy measures (Whittaker, 1972; Riemer and West, 2013; Zhao et al., 2021), three indices, including the average per-particle species diversity D_{α}, the bulk population species diversity D_{γ}, and their affine ratio χ, are calculated to together describe the heterogeneity. The details are described as follows:

Firstly, for the aerosol population with a known κ-PDF with X bins, the volume fraction of the LH and MH components at bin i (i=1, 2, 3, ..., X), $P_{i,\mathrm{LH}}$ and $P_{i,\mathrm{MH}}$, can be calculated by the combination of Eqs. 5 and 6.

$$P_{i,\mathrm{LH}} + P_{i,\mathrm{MH}} = 1, \tag{5}$$

$$P_{i,\mathrm{LH}} \times \kappa_{\mathrm{LH}} + P_{i,\mathrm{MH}} \times \kappa_{\mathrm{MH}} = \kappa_i. \tag{6}$$

Secondly, the mixing entropy for particles at bin i (H_i) can be calculated by

$$H_i = -P_{i,\mathrm{LH}} \times \ln P_{i,\mathrm{LH}} - P_{i,\mathrm{MH}} \times \ln P_{i,\mathrm{MH}}. \tag{7}$$

110 Then the average particle mixing entropy for the aerosol population (H_α) is calculated by

$$H_\alpha = \sum_{ii=1}^{N} P_{ii} \times H_{ii}, \tag{8}$$

where, H_{ii} is the mixing entropy for particle ii (ii=1, 2, 3, ..., N); P_{ii} is the volume proportion of particle ii to the total volume of the aerosol population, which is calculated by

$$P_{ii} = \frac{V_{ii}}{V_{\mathrm{total}}} = \frac{1}{N}, \tag{9}$$

115 because all particles have the same diameters. Considering that particles in the same κ bin have the same physical and chemical properties, they have the same mixing entropy. Eqs.8 and 9 can be simplified as

$$H_\alpha = \sum_{i=1}^{X} \frac{1}{N} \times H_i \times c(\kappa)_i \times \Delta\kappa, \tag{10}$$

where, $c(\kappa)_i$ is the probability density value of κ-PDF at bin i, $\Delta\kappa$ is the bin width.

Additionally, the population-level mixing entropy (H_γ) is calculated by

120 $$H_\gamma = -P_{\mathrm{LH}} \times \ln P_{\mathrm{LH}} - P_{\mathrm{MH}} \times \ln P_{\mathrm{MH}}, \tag{11}$$

where, P_{LH} and P_{MH} are the respective volume fraction of the LH and MH components in the population and calculated by

$$P_{\mathrm{LH}} = \sum_{i=1}^{X} P_{i,\mathrm{LH}} \times c(\kappa)_i \times \Delta\kappa \tag{12}$$

and

$$P_{\mathrm{MH}} = \sum_{i=1}^{X} P_{i,\mathrm{MH}} \times c(\kappa)_i \times \Delta\kappa. \tag{13}$$

125 Thirdly, the per-particle species diversity (D_i), the average per-particle species diversity (D_α) and the population species diversity (D_γ) can be calculated as

$$D_i = e^{H_i},\qquad(14)$$

$$D_\alpha = e^{H_\alpha},\qquad(15)$$

and

130
$$D_\gamma = e^{H_\gamma}.\qquad(16)$$

Finally, a hygroscopic heterogeneity parameter χ can be calculated as

$$\chi = \frac{D_\alpha - 1}{D_\gamma - 1},\qquad(17)$$

which varied from 0% that all particles in the population purely consist of the LH or MH component, to 100% that the LH and MH components are homogeneously distributed in all particles in the population with identical volume fractions.

2.4 Calculation of the size-resolved heterogeneity

A typical four-mode (i. e., a nucleation mode, an Aitken mode, an accumulation mode and a coarse mode) PNSD with a wide size range of 3 nm-10 μm obtained by Ma (2013) is used for the calculation and presentation of the size-resolved heterogeneity. According to the assumption that aerosols in a specific mode have common sources or have experienced similar ageing processes, the corresponding κ_{mean} and κ-PDF of one mode should be the same. The campaign average κ_{mean} and κ-PDF for particles with diameters of 40 nm, 80 nm, and 200 nm measured by H-TDMA are used to deduce the respective κ_{mean} and κ-PDF for the nucleation mode, Aitken mode, and accumulation mode of the fitted PNSDs. κ for the coarse mode is assumed to be 0 because the primary chemical composition in this mode is nearly hydrophobic. Considering the contribution of each mode to the κ_{mean} of specific particle size, the size-resolved κ_{mean} for aerosols ranging from 3 nm-10 μm can be estimated from the known κ_{mean} of each mode ($\kappa_{\mathrm{mean},i}$) as:

145
$$\kappa_{\mathrm{mean}}(D_{\mathrm{p}}) = \frac{\sum_{i=1}^{4} \kappa_{\mathrm{mean},i} \times N_i(D_{\mathrm{p}})}{\sum_{i=1}^{4} N_i(D_{\mathrm{p}})}.\qquad(18)$$

The size-resolved κ-PDF can be calculated using the similar method with Eq. 19:

$$c(\kappa, (D_{\mathrm{p}})) = \frac{\sum_{i=1}^{4} c(\kappa, i) \times \Delta\kappa \times N_i(D_{\mathrm{p}})}{\sum_{i=1}^{4} N_i(D_{\mathrm{p}}) \times \Delta\kappa \times \Delta\log D_{\mathrm{p}}}.\qquad(19)$$

Thus, the size-resolved heterogeneity $D_\alpha(D_{\mathrm{p}})$, $D_\gamma(D_{\mathrm{p}})$, and $\chi(D_{\mathrm{p}})$ for the wide range of 3 nm -10 μm can be obtained by using Eqs. 5-17.

3   Results

3.1   Diagram for particle-to-particle heterogeneity in aerosol hygroscopicity

From the calculation of Eqs. 15-17, D_α can represent the average of the effective number of species existing in each particle and D_γ can represent the effective number of species in the population. Note that $1 \leq D_\alpha \leq D_\gamma$. $D_\alpha = 1$ when all particles are pure while $D_\alpha = D_\gamma$ when all aerosol particles have identical components. The value of D_γ ranges 1 to 2 according to the volume ratio of the LH and MH components in the population. Specifically, it is 1 when the population purely consists of the LH or MH component while 2 when the population has the equivalent volume of the LH and MH components. A triangular region is thus presented in Fig. 2, in which χ is represented by contours and varies from 0% (all particles in the population purely consisted of the LH or MH component, Fig. 2a) to 100% (the LH and MH components are homogeneously distributed in all particles in the population with identical volume fractions, Fig. 2d).

Figs. 2a-2d show an example of the evolution of the heterogeneity in aerosol hygroscopicity. The distributions of the NH and MH components vary between and within populations, causing different heterogeneities for these aerosol populations. Twelve red dots in Fig. 2e represent aerosol populations, each consisting of six aerosol particles with varied fractions of the LH and MH components. Their respective sketch maps and heterogeneity indices are summarized in Table 1, and the corresponding κ-PDFs are listed in Fig. S3 in the supplemental file.

For aerosol populations with particles purely consisting of the LH component or MH component, e. g., populations 1-4, D_α equals 1 and χ equals 0, although D_γ varies from 1 to 2 due to the change of the bulk volume ratio of the LH and MH components. Their κ-PDFs show that κ distributes only at 0.01 for the LH component or 0.6 for the MH component due to the pure component in each particle.

For aerosol populations with equal bulk volume fractions of the LH and MH components, e. g., populations 4-7 and populations 12-10, D_γ has constant values of 2 and 1.5, respectively. The heterogeneous distribution of the LH and MH components contributes to relatively dispersive κ-PDF, with lower D_α and χ. While the homogeneous distribution of these two components, in which all particles have equal amounts of the LH and MH components, leads to a very narrow κ-PDF, and thus higher D_α and χ.

For aerosol populations consisting of particles with identical volume fractions, e. g., populations 7-10, equal values of D_α and D_γ for each population result in χ of 1, although the bulk ratio of the LH to MH components changes between populations. Accordingly, their κ-PDFs are concentrated at a single value of κ_{mean}.

From the populations, it can be concluded that the particle-to-particle heterogeneity in hygroscopicity resulting from the distribution discrepancy of the LH and MH components within particles can be quantified according to the κ-PDF using the proposed algorithm of this work, which can help the heterogeneity to be considered in the calculation of aerosol climate-relevant properties.

3.2 Evolution of the heterogeneity in the real atmosphere

In this section, we apply the proposed algorithm to the in-situ measurement of H-TDMA that was implemented for two periods in 2019 located in Chengdu, China and show the variation characteristic of D_α, D_γ, and χ in the real atmosphere. In the following, the expression of κ-PDF is equivalent to the probability distribution function of g (g-PDF) due to their one-to-one

185 corresponding relationship. Two episodes with tiny changes of κ_{mean} during the observation periods, showing typical evolution processes for 110 nm aerosol populations are chosen and shown in Fig. 3. The first episode appeared from 22:00 (LST) January 13, 2019 to 08:00 (LST) January 14, 2019, and the other one occurred from 00:00 January 27, 2019 to 12:00 January 27, 2019. These two episodes showed that the existing aged aerosol populations with unimodal distributions of κ-PDF, which indicate the uniformly distributed LH and MH components among particles and thus relatively high χ (0.831 for episode 1 at 22:00

190 and 0.832 for episode 2 at 00:00), were intruded by the fresh emissions during the night as reflected by the bimodal and wider distribution of κ-PDF (Yuan et al., 2020). This process led to component discrepancies among particles in populations and thus the decrease of D_α and χ during the midnight.

The statistical PDF of D_α, D_γ, and χ for aerosols with five measured diameters are shown in Fig. 4. The patterns of the distributions for D_α and D_γ move to larger values with increasing diameter, indicating that the effective number of species

195 increases in aerosols with larger diameter due to the longer aging time in the atmosphere. This trend is more obvious in summer campaign. Taking the aerosols of 110 nm for example, D_α varies between 1.386 and 1.850, and D_γ varies between 1.470 and 2.000 during the winter field measurements. The ranges of D_α and D_γ in summer are 1.280-1.928 and 1.371-2.000, respectively, contributing to a wider distribution of χ. This indicates that the fraction of the LH and MH components varied more pronounced due to the complex aging processes in summer compared to that in winter. χ ranging from 0.6 to 0.9 reveals

200 the large variation of heterogeneity in aerosol hygroscopicity in the real atmosphere.

In short, the algorithm proposed in this work can efficiently characterize the evolution of aerosol heterogeneity with time in the real atmosphere and provides an unexplored understanding of the H-TDMA measurement.

3.3 Importance of the heterogeneity in aerosol hygroscopicity

The same bulk volume fraction of the LH and MH components indicates the same κ_{mean} for populations (e.g., populations 4-7

205 and populations 10-12). This reveals the identical diameter for all particles in each population after hygroscopic growth at high RH. Actually, due to the particle-to-particle heterogeneity in one population, different ratios of the LH and MH components in each particle result in different κ (e. g., particles in each of populations 4-7), which can lead to different ambient number size distributions, especially for the condition with high RH. Fig. 5 depicts a sample of the hygroscopic size distribution, where RH is 90%, for three aerosol populations with the same κ_{mean} of 0.305 but different χ of 0.653, 0.884, and 0.999, respectively.

210 Each of these three populations contains 1000 aerosol particles with dry diameters of 100 nm. Significant discrepancies can be seen in the number size distribution that the width decreases while the peak value increases with increasing χ after hygroscopic growth. Thus, the heterogeneity in aerosol hygroscopicity plays a significant role in the evolution of aerosol ambient number size distributions, which is a key factor for evaluating aerosol radiative forcing.

3.4 Size-resolved heterogeneity in aerosol hygroscopicity

215 The heterogeneity for only one size can contribute to dramatically different ambient size distributions, especially for the condition under high RH. Thus, it is urgently needed to figure out how the heterogeneity varies with aerosol size in the real atmosphere. This section will discuss the characteristic of the size-resolved heterogeneity in aerosol hygroscopicity.

PNSD within the range of 3 nm-10 μm is commonly observed by commercial instruments, including the scanning mobility particle sizer (SMPS) and the Wide Range Particle Spectrometer (WPS) around the world (Wu and Boor, 2021). However, the
220 widely used H-TDMA technic can only observe the growth factor of aerosols with limited sizes (generally smaller than 350 nm in the dry condition), e. g., 40, 80, 110, 150, and 200 nm in this study. Recently, Shen et al. (2021) extended the H-TDMA measurement of aerosol hygroscopic properties to 600 nm in the urban environment. Although κ for larger particles (> 1 μm) can be derived from the size-resolved chemical composition (Liu et al., 2014; Gysel et al., 2007), the size-resolved κ with high size and time resolution is scarce and is needed to be observed or reversed by more advanced technology and new algorithms.
225 Fortunately, Chen et al. (2012) provided an approach to derive the size-resolved κ for aerosols within the range of 3 nm-10 μm based on the measured PNSDs and H-TDMA determined κ. They used the κ_{mean} for each measured size by neglecting aerosol heterogeneity. Here, the heterogeneity in aerosol hygroscopicity is considered based on the method provided by Chen et al. (2012) (Methods section).

The typical four-mode PNSD mentioned above is used and shown in Fig. 6a and Fig. 6d. The κ_{mean} and the corresponding
230 κ-PDFs for the nucleation mode, Aitken mode, and accumulation mode are represented by those measured at sizes of 40 nm, 80 nm, and 200 nm, respectively, during the winter (Fig. 6b) and summer (Fig. 6e) campaigns. The calculated size-resolved κ_{mean} are shown in Fig. 6c (winter) and Fig. 6f (summer), in which κ-PDF for each size contributed by the heterogeneity in aerosol hygroscopicity is represented by the contour. The variation of both the size-resolved κ_{mean} and the corresponding κ-PDF are influenced by the contribution of each mode to the total number concentration. The corresponding χ for the size
235 range of 3 nm-10 μm can therefore be calculated by using the framework proposed by this work.

As shown in Fig. 6, the consideration of the heterogeneity provides the size-resolved κ-PDF, which can further show the region where the κ is mostly distributed for aerosol populations of any size and how aerosols evolve with size in the population. For example, although κ_{mean} for aerosol populations smaller than 40 nm is 0.131 during the winter campaign, the κ-PDF shows most κ locate at a narrow area lower than 0.05. The continuous evolution of the κ-PDF with sizes smaller than 1 μm indicates
240 that on the one hand, a part of the aerosols in the population has increasing hygroscopicity during the aging process of growing up, which is the main reason for the increase of κ_{mean}, on the other hand, NH-dominated aerosols exist across all sizes. This corresponds to the slight decreasing trend of χ accompanied by a wider area of κ ranging from 0.01 to larger than 0.4, which reflects the heterogeneous distribution of the LH and MH components between aerosol particles within a population during the aging progress.
245 Additionally, the phenomenon that a sharp decrease of χ close to 0.1 for aerosol populations larger than 1 μm and the κ-PDFs for this size range shows a very narrow band lying at κ of 0 responds to the assumption that the coarse mode particle is mainly composed of the NH component.

Overall, this newly developed aerosol heterogeneity provides more insight into the evolution of aerosol populations during the aging processes. The hygroscopicity of an aerosol population is complicated and diverse due to the particle-to-particle heterogeneity in aerosol hygroscopicity, if only the κ_{mean} is applied without considering aerosol heterogeneity, significant uncertainty will occur.

4   Conclusions

The particle-to-particle heterogeneity in aerosol hygroscopicity is of great importance for better understanding the impact of hygroscopicity on estimating aerosol climatic and environmental effects. Unfortunately, the heterogeneity has not been paid attention to in previous studies, of which only the population-averaged hygroscopicity parameter, κ_{mean}, is considered, mainly because the heterogeneity is difficult to be quantified in both observations and models.

In this work, we proposed an algorithm to quantify the particle-to-particle heterogeneity in aerosol hygroscopicity from the in-situ measurement for the first time. This algorithm is an innovation on the basis of the mature theory in information-theoretic entropy and the widely used assumption that aerosol populations are binary systems consisting of the commonly defined LH and MH components from H-TDMA measurement.

Three indices, including the average per-particle species diversity D_{α}, the bulk population species diversity D_{γ}, and their affine ratio χ, are calculated from the probability distribution of κ to together describe aerosol heterogeneity. They can efficiently characterize and provide more insight into the evolution of aerosol heterogeneity with time in the real atmosphere during the aging processes.

The heterogeneity varies much with aerosol particle size and large discrepancies can be seen in aerosol particle number size distribution (PNSD) that the width decreases while the peak value of the PNSD increases with increasing χ after hygroscopic growth, especially for conditions with high relative humidity, indicating the vital role of the heterogeniety in the evolution of ambient PNSD.

Considering that PNSD is a key factor for the evaluation of aerosol impacts on radiative forcing, significant uncertainties will occur in calculating the climate-relevant properties if the population-averaged hygroscopicity is applied by neglecting its heterogeneity. Thus, the particle-to-particle heterogeneity in aerosol hygroscopicity is urgently needed to be represented in models. This work, which has the intuitive and quantitative interpretation of aerosol heterogeneity, sheds light on the importance and provides a framework of merging observations into numerical models to deeply investigate how heterogeneity in aerosol hygroscopicity influences aerosol effects on climate and environment.

Data availability.   The data is available at https://doi.org/10.5281/zenodo.7320916.

Author contributions.   C.Z. designed the research project and reviewed the manuscript. L.Y. interpreted all results and contributed to writing.

Competing interests. The authors declare no competing interests.

Acknowledgements. The authors acknowledge Yuzhang Che, Pengguo Zhao, Jinhui, Gao, and Hui Xiao for fruitful discussions. This work is supported by the National Science Foundation of China (NSFC) (42005072 and 42075086) and the Open Project of Key Laboratory for 280 Aerosol-Cloud-Precipitation of China Meteorological Administration, NUIST (KDW1903).

References

Bian, Y., Zhao, C., Ma, N., Chen, J., and Xu, W.: A study of aerosol liquid water content based on hygroscopicity measurements at high relative humidity in the North China Plain, Atmospheric Chemistry and Physics, 14, 6417–6426, https://doi.org/10.5194/acp-14-6417-2014, 2014.

285 Brock, C. A., Wagner, N. L., Anderson, B. E., Attwood, A. R., Beyersdorf, A., Campuzano-Jost, P., Carlton, A. G., Day, D. A., Diskin, G. S., Gordon, T. D., et al.: Aerosol optical properties in the southeastern United States in summer–Part 1: Hygroscopic growth, Atmospheric Chemistry and Physics, 16, 4987–5007, https://doi.org/10.5194/acp-16-4987-2016, 2016.

Cai, M., Tan, H., Chan, C. K., Qin, Y., Xu, H., Li, F., Schurman, M. I., Liu, L., and Zhao, J.: The size-resolved cloud condensation nuclei (CCN) activity and its prediction based on aerosol hygroscopicity and composition in the Pearl Delta River (PRD) region during wintertime

290 2014, Atmospheric Chemistry and Physics, 18, 16 419–16 437, https://doi.org/10.5194/acp-18-16419-2018, 2018.

Chen, J., Zhao, C., Ma, N., Liu, P., Göbel, T., Hallbauer, E., Deng, Z., Ran, L., Xu, W., Liang, Z., et al.: A parameterization of low visibilities for hazy days in the North China Plain, Atmospheric Chemistry and Physics, 12, 4935–4950, https://doi.org/10.5194/acp-12-4935-2012, 2012.

Chen, J., Zhao, C., Ma, N., and Yan, P.: Aerosol hygroscopicity parameter derived from the light scattering enhancement factor measurements

295 in the North China Plain, Atmospheric Chemistry and Physics, 14, 8105–8118, https://doi.org/10.5194/acp-14-8105-2014, 2014.

Drucker, J.: Industrial structure and the sources of agglomeration economies: evidence from manufacturing plant production, Growth and Change, 44, 54–91, https://doi.org/10.1111/grow.12002, 2013.

Falush, D., Stephens, M., and Pritchard, J. K.: Inference of population structure using multilocus genotype data: dominant markers and null alleles, Molecular ecology notes, 7, 574–578, https://doi.org/10.1111/j.1471-8286.2007.01758.x, 2007.

300 Fierce, L., Bond, T. C., Bauer, S. E., Mena, F., and Riemer, N.: Black carbon absorption at the global scale is affected by particle-scale diversity in composition, Nature communications, 7, 1–8, https://doi.org/10.1038/ncomms12361, 2016.

Fierce, L., Onasch, T. B., Cappa, C. D., Mazzoleni, C., China, S., Bhandari, J., Davidovits, P., Fischer, D. A., Helgestad, T., Lambe, A. T., et al.: Radiative absorption enhancements by black carbon controlled by particle-to-particle heterogeneity in composition, Proceedings of the National Academy of Sciences, 117, 5196–5203, https://doi.org/10.1073/pnas.1919723117, 2020.

305 Gysel, M., Crosier, J., Topping, D., Whitehead, J., Bower, K., Cubison, M., Williams, P., Flynn, M., McFiggans, G., and Coe, H.: Closure study between chemical composition and hygroscopic growth of aerosol particles during TORCH2, Atmospheric Chemistry and Physics, 7, 6131–6144, https://doi.org/10.5194/acp-7-6131-2007, 2007.

Gysel, M., McFiggans, G., and Coe, H.: Inversion of tandem differential mobility analyser (TDMA) measurements, Journal of Aerosol Science, 40, 134–151, https://doi.org/10.1016/j.jaerosci.2008.07.013, 2009.

310 Köhler, H.: The nucleus in and the growth of hygroscopic droplets, Transactions of the Faraday Society, 32, 1152–1161, https://doi.org/10.1039/tf9363201152, 1936.

Kuang, Y., Zhao, C., Tao, J., Bian, Y., Ma, N., and Zhao, G.: A novel method for deriving the aerosol hygroscopicity parameter based only on measurements from a humidified nephelometer system, Atmospheric Chemistry and Physics, 17, 6651–6662, https://doi.org/10.5194/acp-17-6651-2017, 2017.

315 Liu, B., Pui, D., Whitby, K., Kittelson, D. B., Kousaka, Y., and McKenzie, R.: The aerosol mobility chromatograph: a new detector for sulfuric acid aerosols, Atmospheric Environment, pp. 99–104, https://doi.org/10.1016/0004-6981(78)90192-0, 1978.

Liu, H., Zhao, C., Nekat, B., Ma, N., Wiedensohler, A., Van Pinxteren, D., Spindler, G., Müller, K., and Herrmann, H.: Aerosol hygroscopicity derived from size-segregated chemical composition and its parameterization in the North China Plain, Atmospheric Chemistry and Physics, 14, 2525–2539, https://doi.org/10.5194/acp-14-2525-2014, 2014.

320 Liu, P., Zhao, C., Göbel, T., Hallbauer, E., Nowak, A., Ran, L., Xu, W., Deng, Z., Ma, N., Mildenberger, K., et al.: Hygroscopic properties of aerosol particles at high relative humidity and their diurnal variations in the North China Plain, Atmospheric Chemistry and Physics, 11, 3479–3494, https://doi.org/10.5194/acp-11-3479-2011, 2011.

Liu, X. G., Li, J., Qu, Y., Han, T., Hou, L., Gu, J., Chen, C., Yang, Y., Liu, X., Yang, T., Zhang, Y., Tian, H., and Hu, M.: Formation and evolution mechanism of regional haze: a case study in the megacity Beijing, China, Atmospheric Chemistry and Physics, 13, 4501–4514,

325 https://doi.org/10.5194/acp-13-4501-2013, 2013.

Ma, N.: Aerosol optical and activation properties in the North China Plain, Peking University, 2013.

Petters, M. and Kreidenweis, S.: A single parameter representation of hygroscopic growth and cloud condensation nucleus activity, Atmospheric Chemistry and Physics, 7, 1961–1971, https://doi.org/10.5194/acp-7-1961-2007, 2007.

Riemer, N. and West, M.: Quantifying aerosol mixing state with entropy and diversity measures, Atmospheric Chemistry and Physics, 13,

330 11 423–11 439, https://doi.org/10.5194/acp-13-11423-2013, 2013.

Shen, C., Zhao, G., Zhao, W., Tian, P., and Zhao, C.: Measurement report: aerosol hygroscopic properties extended to 600 nm in the urban environment, Atmospheric Chemistry and Physics, 21, 1375–1388, https://doi.org/10.5194/acp-21-1375-2021, 2021.

Stokes, R. and Robinson, R.: Interactions in aqueous nonelectrolyte solutions. I. Solute-solvent equilibria, The Journal of Physical Chemistry, 70, 2126–2131, https://doi.org/10.1021/j100879a010, 1966.

335 Stolzenburg, M. R. and McMurry, P. H.: Equations governing single and tandem DMA configurations and a new lognormal approximation to the transfer function, Aerosol Science and Technology, 42, 421–432, https://doi.org/10.1080/02786820802157823, 2008.

Strong, S. P., Koberle, R., Van Steveninck, R. R. D. R., and Bialek, W.: Entropy and information in neural spike trains, Physical review letters, 80, 197, https://doi.org/10.1103/PhysRevLett.80.197, 1998.

Swietlicki, E., Hansson, H.-C., Hämeri, K., Svenningsson, B., Massling, A., McFiggans, G., McMurry, P., Petäjä, T., Tunved, P., Gysel,

340 M., et al.: Hygroscopic properties of submicrometer atmospheric aerosol particles measured with H-TDMA instruments in various environments—a review, Tellus B: Chemical and Physical Meteorology, 60, 432–469, https://doi.org/10.1111/j.1600-0889.2008.00350.x, 2008.

Tan, H., Xu, H., Wan, Q., Li, F., Deng, X., Chan, P., Xia, D., and Yin, Y.: Design and application of an unattended multifunctional H-TDMA system, Journal of Atmospheric and Oceanic Technology, 30, 1136–1148, https://doi.org/10.1175/JTECH-D-12-00129.1, 2013a.

345 Tan, H., Yin, Y., Gu, X., Li, F., Chan, P., Xu, H., Deng, X., and Wan, Q.: An observational study of the hygroscopic properties of aerosols over the Pearl River Delta region, Atmospheric Environment, 77, 817–826, https://doi.org/10.1016/j.atmosenv.2013.05.049, 2013b.

Tao, J., Zhao, C., Ma, N., and Liu, P.: The impact of aerosol hygroscopic growth on the single-scattering albedo and its application on the NO_2 photolysis rate coefficient, Atmospheric Chemistry and Physics, 14, 12 055–12 067, https://doi.org/10.5194/acp-14-12055-2014, 2014.

350 Tie, X., Huang, R.-J., Cao, J., Zhang, Q., Cheng, Y., Su, H., Chang, D., Pöschl, U., Hoffmann, T., Dusek, U., et al.: Severe pollution in China amplified by atmospheric moisture, Scientific Reports, 7, 1–8, https://doi.org/10.1038/s41598-017-15909-1, 2017.

Tsimring, L. S., Levine, H., and Kessler, D. A.: RNA virus evolution via a fitness-space model, Physical review letters, 76, 4440, https://doi.org/10.1103/PhysRevLett.76.4440, 1996.

Wang, Y. and Chen, Y.: Significant climate impact of highly hygroscopic atmospheric aerosols in Delhi, India, Geophysical Research Letters, 46, 5535–5545, https://doi.org/10.1029/2019GL082339, 2019.

Wang, Y., Li, Z., Zhang, Y., Du, W., Zhang, F., Tan, H., Xu, H., Fan, T., Jin, X., Fan, X., et al.: Characterization of aerosol hygroscopicity, mixing state, and CCN activity at a suburban site in the central North China Plain, Atmospheric Chemistry and Physics, 18, 11 739–11 752, https://doi.org/10.5194/acp-18-11739-2018, 2018.

Whittaker, R. H.: Evolution and measurement of species diversity, Taxon, 21, 213–251, https://doi.org/10.2307/1218190, 1972.

Wu, T. and Boor, B. E.: Urban aerosol size distributions: a global perspective, Atmospheric Chemistry and Physics, 21, 8883–8914, https://doi.org/10.5194/acp-21-8883-2021, 2021.

Yuan, L., Zhang, X., Feng, M., Liu, X., Che, Y., Xu, H., Schaefer, K., Wang, S., and Zhou, Y.: Size-resolved hygroscopic behaviour and mixing state of submicron aerosols in a megacity of the Sichuan Basin during pollution and fireworks episodes, Atmospheric Environment, 226, 117 393, https://doi.org/10.1016/j.atmosenv.2020.117393, 2020.

Zdanovskii, A.: New methods for calculating solubilities of electrolytes in multicomponent systems, Zh. Fiz. Khim, 22, 1478–1485, 1948.

Zhao, G., Tan, T., Zhu, Y., Hu, M., and Zhao, C.: Method to quantify black carbon aerosol light absorption enhancement with a mixing state index, Atmospheric Chemistry and Physics, 21, 18 055–18 063, https://doi.org/10.5194/acp-21-18055-2021, 2021.

Zieger, P., Fierz-Schmidhauser, R., Weingartner, E., and Baltensperger, U.: Effects of relative humidity on aerosol light scattering: results from different European sites, Atmospheric Chemistry and Physics, 13, 10 609–10 631, https://doi.org/10.5194/acp-13-10609-2013, 2013.
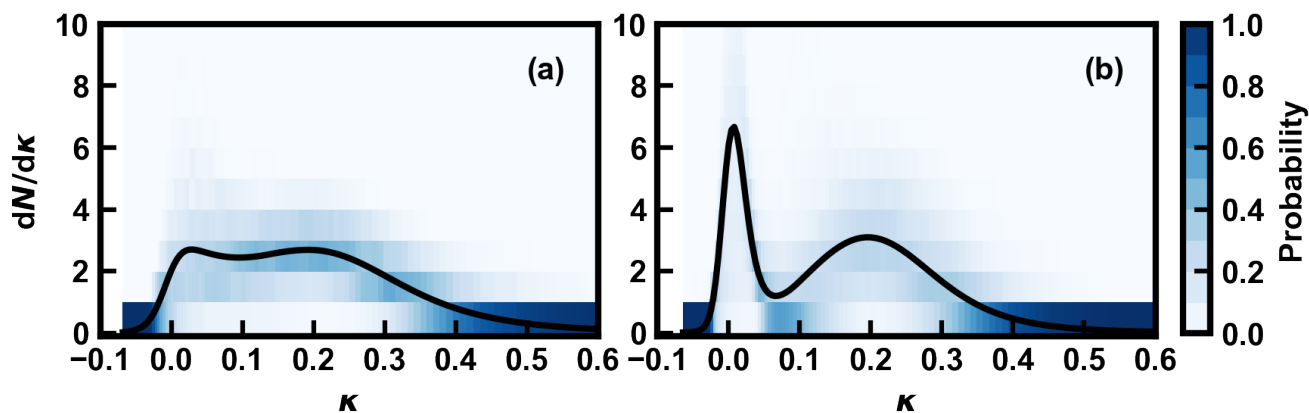
Figure 1. Typical κ-PDF for 100 nm aerosols in winter (a) and summer (b) measured by H-TDMA over Chengdu. The shaded is the frequency distribution of κ-PDF, and the solid lines show the campaign average of κ-PDF.
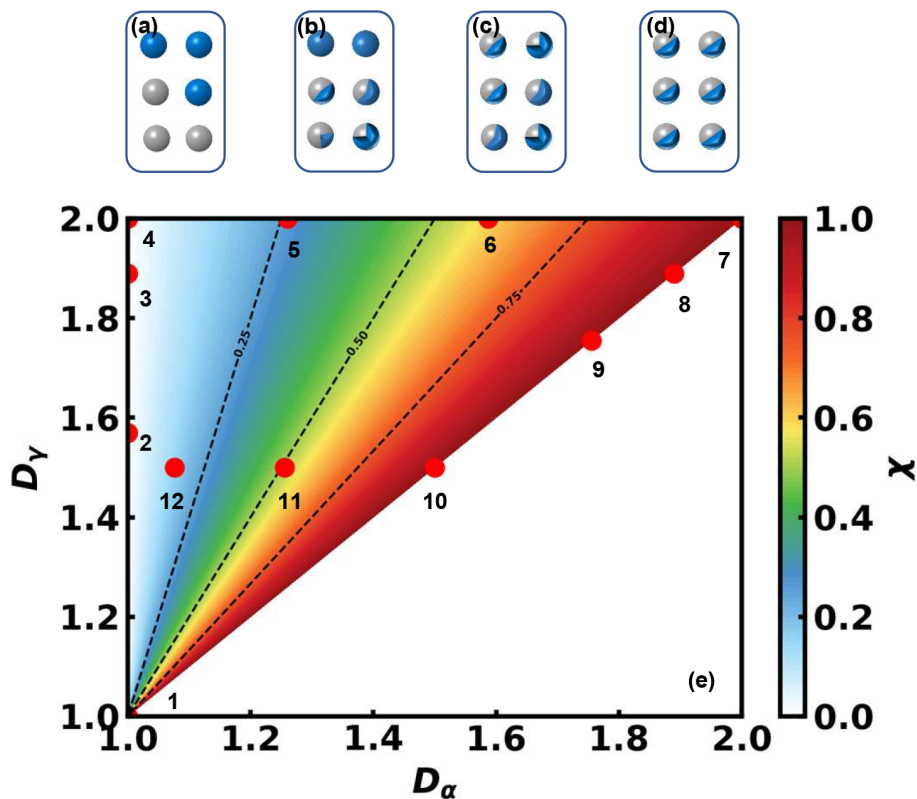
Figure 2. Example of the evolution of the heterogeneity in aerosol hygroscopicity (a-d) and diagram for the relationship among D_α, D_γ, and χ (e). Twelve different aerosol populations, each of which consists of six particles as shown in Table 1, are represented by the red points.
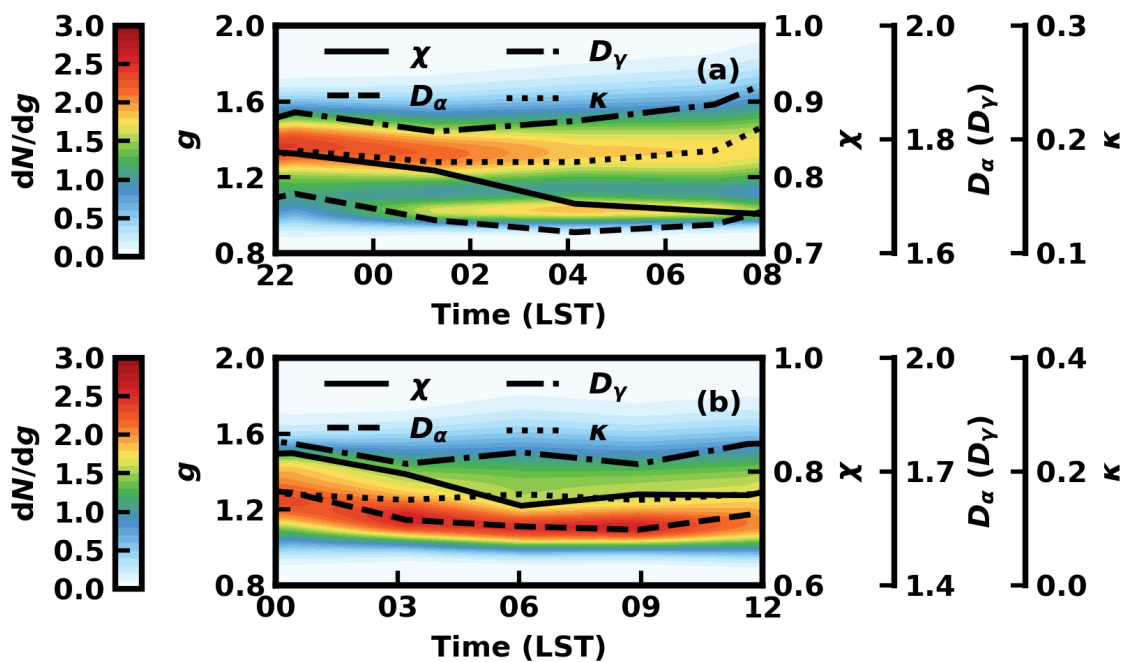
Figure 3. The variation of D_α, D_γ, and χ during two typical evolution processes for 110 nm aerosol populations with tiny changes of κ_{mean} on January 13, 2019 (a) and January 27, 2019 (b).
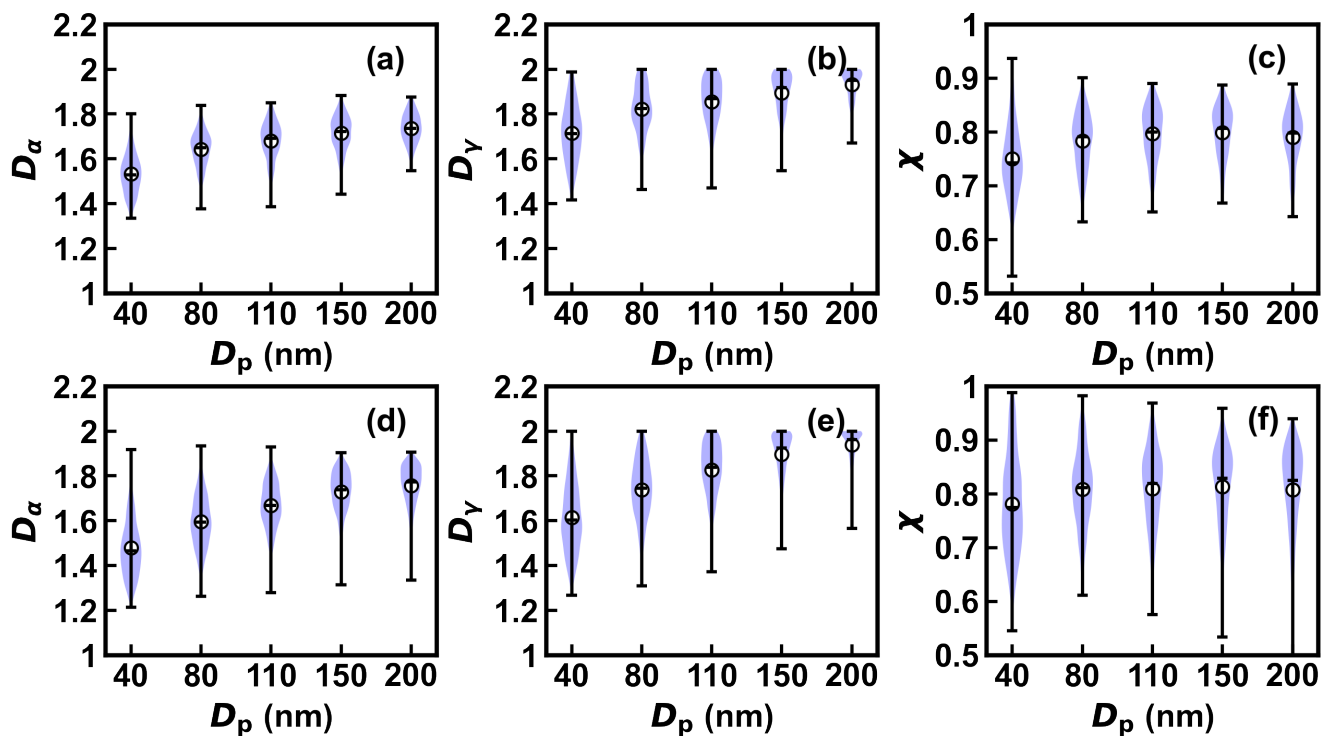
Figure 4. The statistical of D_α, D_γ, and χ for aerosol populations of five measured diameters in winter (a), (b), (c) and summer (d), (e), (f). The shaded is the frequency distribution of the indices. The three bars on whisker for each diameter from the bottom to the top are the minimum, median, and maxmum, and the circles represent the average of the indices.
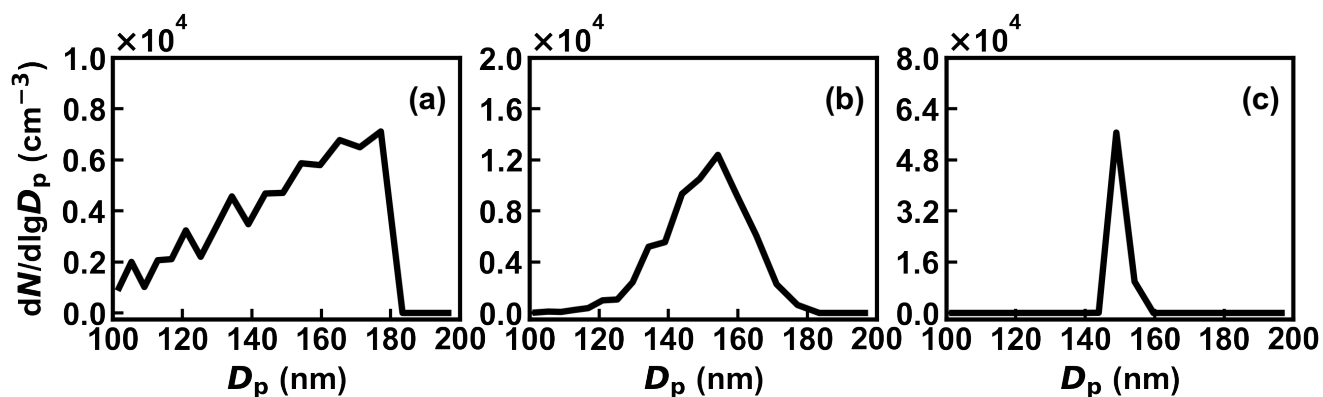
Figure 5. Aerosol particle size distributions after hygroscopic growth at RH of 90% for three aerosol populations with χ of 0.653 (a), 0.884 (b), and 1 (c), respectively. Each of these three populations has the same κ_{mean} of 0.305 and contains 1000 aerosol particles with dry diameters of 100 nm.
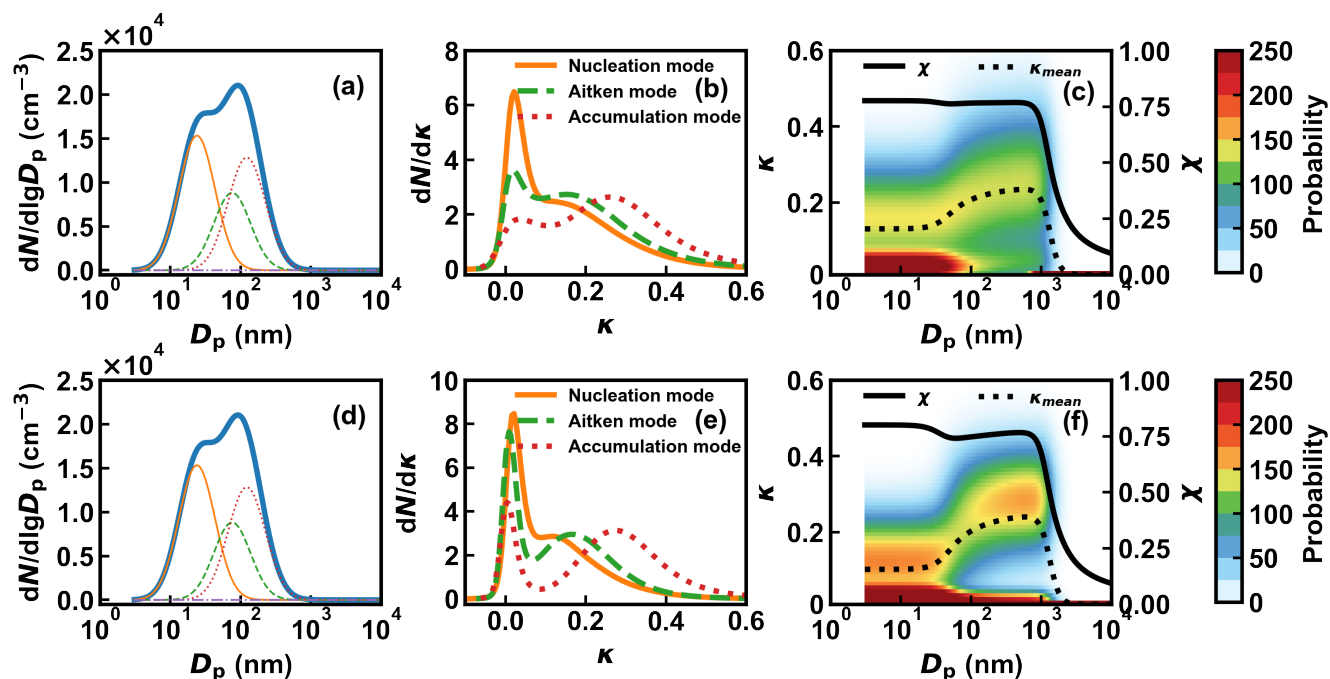
Figure 6. The typical PNSD (a), (d) and the κ-PDF during the winter (b) and summer campaigns (e) used for calculating the size-resolve κ_{mean}, the size-resolved κ-PDF, and the corresponding size-resolved χ (c), (f). The solid lines (blue) in (a) and (d) are the measured PNSD that can be fitted by a four-mode (a nucleation mode, an Aitken mode, an accumulation mode and a coarse mode) lognormal distribution, which are represented by the thin solid line (orange), the dashed line (green), the dotted line (red), and the dash-dotted line (purple), respectively. The corresponding type and color lines represent the the measured campaign average κ-PDF for each mode. The dot line in (c) and (f) is the calculated size-resolve κ_{mean}, and the color shaded is the corresponding size-resolved κ-PDF. The solid lines in (c) and (f) is the calculated size-resolved χ.

Table 1. The sketch map of the components and the corresponding indices for the 12 different aerosol populations in Fig. 2. The LH and MH components are represented by the colors of blue and gray, respectively, V_{LH} and V_{MH} represent their volumes.

Pop.	Sketch map	$V_{\mathrm{LH}}:V_{\mathrm{MH}}$	D_α	D_γ	χ	κ_{mean}
1	or	0:6 or 6:0	1	1	0	0.6 or 0.01
2	or	1:5 or 5:1	1	1.569	0	0.502 or 0.108
3	or	1:2 or 2:1	1	1.890	0	0.403 or 0.207
4		1:1	1	2	0	0.305
5		1:1	1.260	2	0.260	0.305
6		1:1	1.587	2	0.587	0.305
7		1:1	2	2	1	0.305
8	or	1:2 or 2:1	1.890	1.890	1	0.403 or 0.207
9	or	1:3 or 3:1	1.760	1.760	1	0.451 or 0.159
10	or	1:6.13 or 6.13:1	1.500	1.500	1	0.517 or 0.093
11	or	1:6.13 or 6.13:1	1.260	1.500	0.510	0.517 or 0.093
12	or	1:6.13 or 6.13:1	1.076	1.500	0.151	0.517 or 0.093